Electronic Supplementary Material (ESI) for Journal of Materials Chemistry A.

Electronic Supplementary Information

Novel Sea Cucumber-Inspired Materials Constructed Based on Stiff, Strong yet Tough Elastomer Demonstrating Unique Self-healing and Recyclable Functionalities

JianHua Xu, Sheng Ye and JiaJun Fu*

School of Chemical Engineering, Nanjing University of Science and Technology, Nanjing, 210094, People's Republic of China.

***Corresponding author. E-mail: fujiajun668@gmail.com**

Table of Contents

Materials and methods....3
Synthesis and polymerization....4
Synthesis of polymeric monomers....4
Polymerization of HHIF material....7
Formation of HHIF-Zn material....7
Bulk characterization....8
Relative humidity control....8
Mechanical tests....9
Self-healing tests....9
Supplementary figure....10
Supplementary Table....16
Supplementary movie....17
Reference....18

Materials and method

1,1'-(Methylenedi-4,1-phenylene) bismaleimide (Bis-MM, 98%) was purchased from Sigma-Aldrich. 2,2-Azobis(2-methylpropionitrile) (AIBN, 99%) and triethylamine (99%) were supplied by J&K Scientific. Furfural alcohol (FA, 98%) and sodium bicarbonate (>99.8%) and were purchased from Macklin. 1-(3-amipropyl) imidazole (IMD-NH_2, 98%) and acryloyl chloride (AC, 98%) were supplied by Alfa Aesar. 2-Hydroxyethyl acrylate (HEA, 97%) and Zinc trifluoromethanesulfonate (98%, $Zn(OTf)_2$) were purchased from Aladdin (Shanghai, China). The $Zn(OTf)_2$ metal salts were stored and weighted in a nitrogen atmosphere glove box to minimize water absorption and ensure accurate measurements. N,N-Dimethylformamide (DMF), dichloromethane and toluene were dried with the molecular sieves for 24 h before use. Water used in all the experiments was obtained via a Milli-Q water system with a resistivity of 18.0 MΩ cm.

^1H NMR spectra were recorded on a Bruker ADVANCE 300 spectrometer at 300 MHz. Mass spectra was recorded on a Thermo Trace DSQ LC-MS spectrometer.

Synthesize and polymerization

Synthesis of polymeric monomers

Synthesis of compound 1 (Bis-DA-OH)

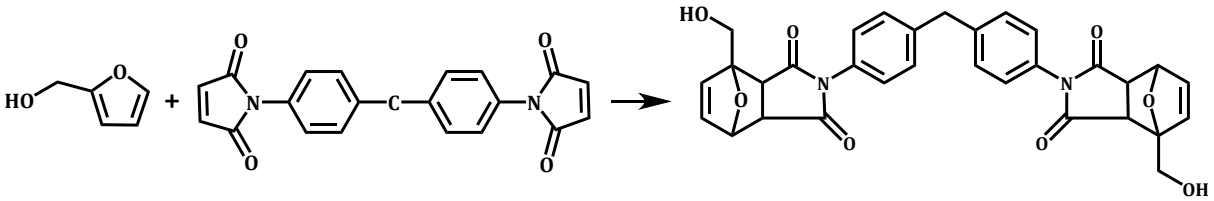

0.75 g (2 mmol) of Bis-MM and 0.4 g (4 mmol) of FA were dissolved in 20 mL toluene at room temperature. Then, the reaction temperature was gradually increased to 60 °C and the mixed solution was further stirred for 12 h to trigger Diels-Alder reaction, resulting in a large number of precipitates. Subsequently, the filtered precipitates were dissolved in 5 mL dichloromethane to obtain yellow clear solution. The obtained solution was injected dropwise into diethyl ether and the liquid was removed by filtration to obtain the precipitates. After that, the precipitates were further washed with diethyl ether (200 mL) and dried in vacuum. Yield: 0.92 g, 80%.

^{1}H NMR (300 MHz, DMSO-d6, 298 K): δ (ppm) 7.31 (d, *J*=4.5 Hz, 4H), 7.08 (d, *J*=4.5 Hz, 4H), 6.53 (s, 4H), 5.14 (s, 2H), 4.97 (t, *J*=3.24 Hz, 2H), 4.00 (m, 4H), 3.16 (d, *J*=3.9 Hz, 2H), 2.98 (d, J=3.9 Hz, 2H).

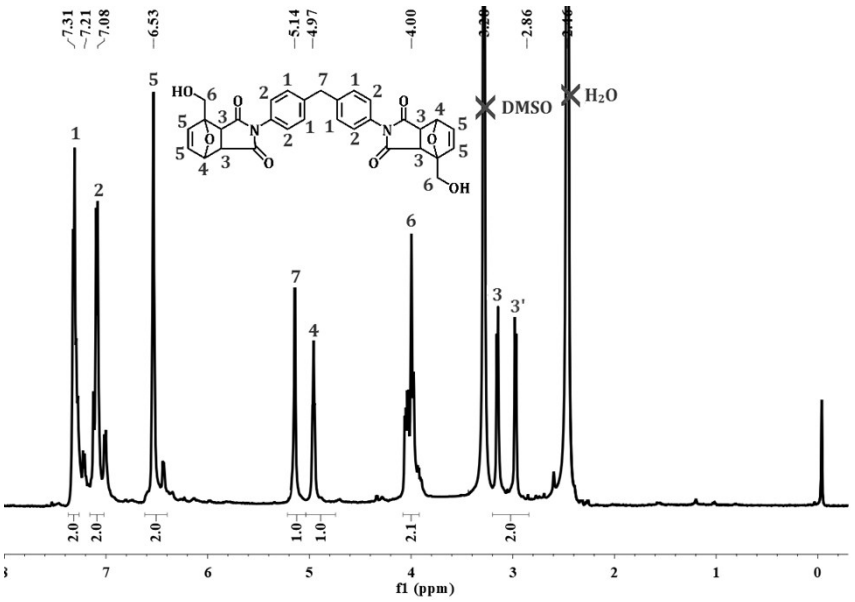

Fig. S1 ^{1}H NMR spectrum for Bis-DA-OH (300 MHz, DMSO-d6, 298 K).

Synthesis of compound 2 (FMDA)

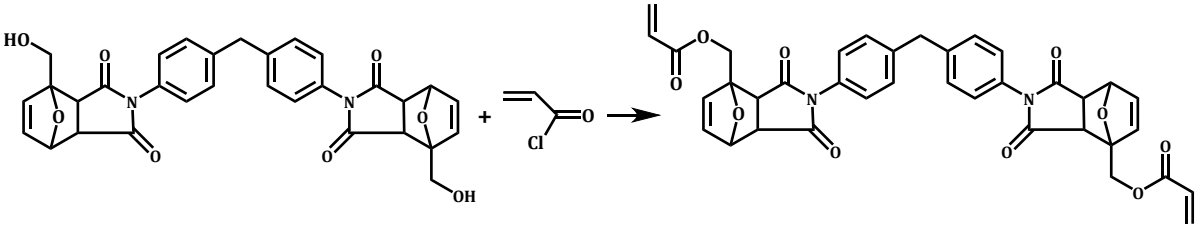

A solution of Bis-DA-OH (1.0 g, 1.8 mmol) in dichloromethane (10 mL) was cooled to 0 °C under nitrogen atmosphere. Then, 2 mL (14 mmol) of triethylamine was added and the mixed solution was stirred for 10 min. After that, 0.6 g (6 mmol) of acryloyl chloride was injected dropwise and a gas formation was observed. Subsequently, this mixed solution was stirred at 0 °C for 1 h, and then warmed to room temperature for further reaction for 24 h. Finally, the generated triethylamine hydrochloride was removed by filtration. The obtained filter liquor was poured into diethyl ether (200 mL) and the liquid phase was removed by filtration. The precipitates were dried in vacuum to get purified product. Yield: 1.31 g, 82%.

^{1}H NMR (300 MHz, DMSO-d6, 298 K): δ (ppm) 7.35 (d, *J*=7.38 Hz, 4H), 7.15 (d, J=7.38 Hz, 4H), 6.66-6.52 (m, 4H), 6.37-5.76 (m, 6H), 5.25-4.84 (m, 2H), 4.51 (d, *J*=13.14 Hz, 2H), 4.04 (s, 4H), 3.24 (d, *J*=6.6 Hz, 2H), 3.18 (d, *J*=6.6 Hz, 2H).

Note that the retro-Diels-Alder reaction could take place during the MS testing process. Thus we cannot employ this method to determine the mass of Bis-DA-OH and FMDA.

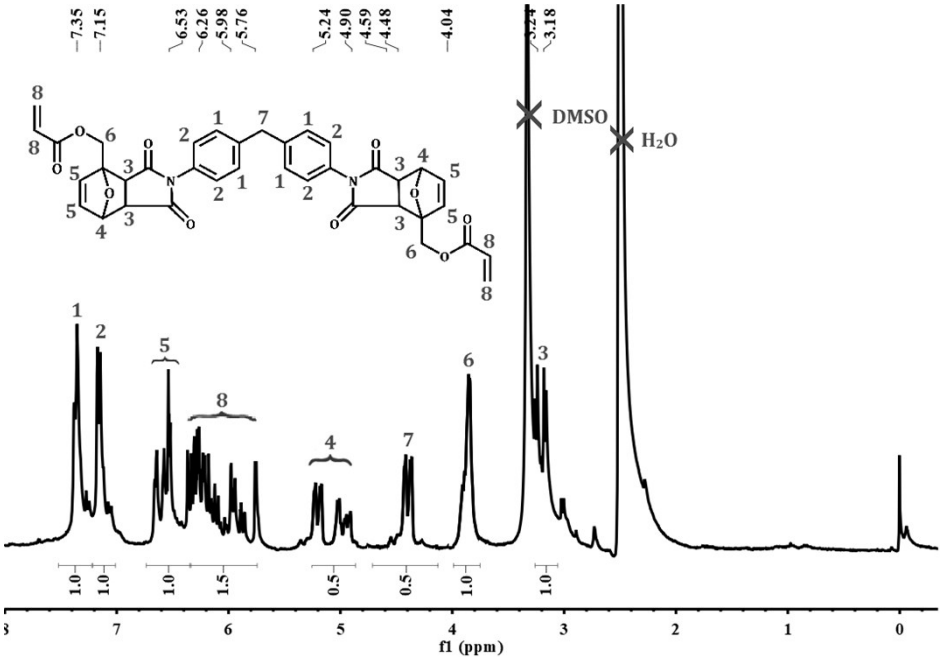

Fig. S2 ^{1}H NMR spectrum for FMDA (300 MHz, DMSO-d6, 298 K).

Synthesis of compound 3 (IMPAA)

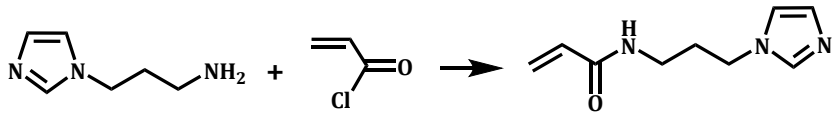

A solution of 1-(3-Aminopropyl) imidazole (1.6 g, 13 mmol) in 5 mL ultrapure water was cooled to 0 ℃ under nitrogen atmosphere. Subsequently, 1.4 g (16 mmol) of sodium bicarbonate was added and stirred for 10 min. After that, 1.14 g (0.016 mol) of acryloyl chloride was injected dropwise into the above solution. The mixed solution was stirred at 0 ℃ for 1 h, and then the reaction temperature was gradually increased to room temperature for further 15 h reaction. At the end of the reaction, the salt precipitate in solution was removed by filtration. The filtrate was washed with 50 mL trichloromethane, and then the organic phase was dried over anhydrous Na_2SO_4. After that, Na_2SO_4 was removed via filtration and the excess solution was removed by reduced pressure distillation. The product was purified by column chromatography (methanol/dichloromethane on silica, 1:3, v/v). Yield: 1.20 g, 40%.

^{1}H NMR (300 MHz, $CDCl_3$, 298 K): δ (ppm) 7.44 (s, 1H), 7.03 (s, 1H), 6.95 (s, 1H), 6.30 (d, *J*=10.29 Hz, 1H, double bond), 6.13 (dd, *J*=6.18 Hz, 4.08 Hz, 1H), 5.64 (d, *J*=6.03 Hz, 1H, double bond), 4.00 (t, *J*=3.87 Hz, 2H), 3.33 (q, *J*=4.05 Hz, 2H), 2.04 (m, *J*=4.17 Hz, 2H). **MS (ESI):** m/z calcd. For $C_9H_{13}N_3O$: 179.11; found: 179.91 $[M+H]^+$.

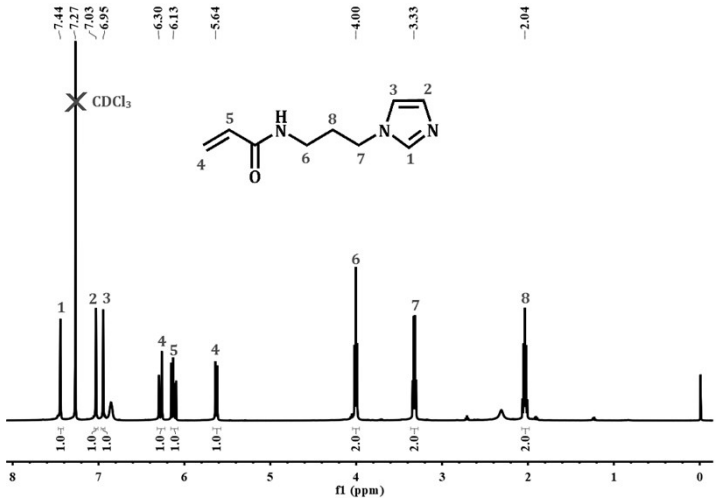

Fig. S3 ^{1}H NMR spectra for IMPAA (300 MHz, $CDCl_3$, 298 K).

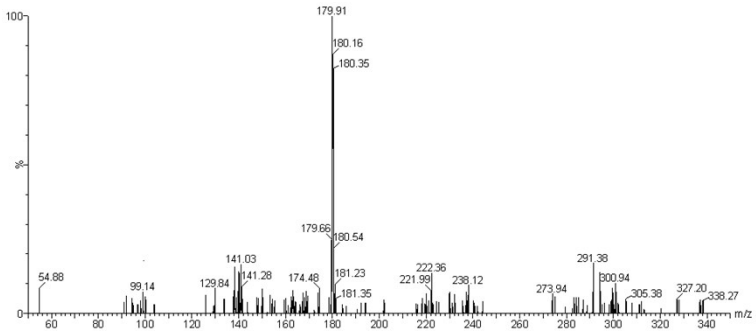

Fig. S4 MS spectra for IMPAA .

Polymerization of HHIF material

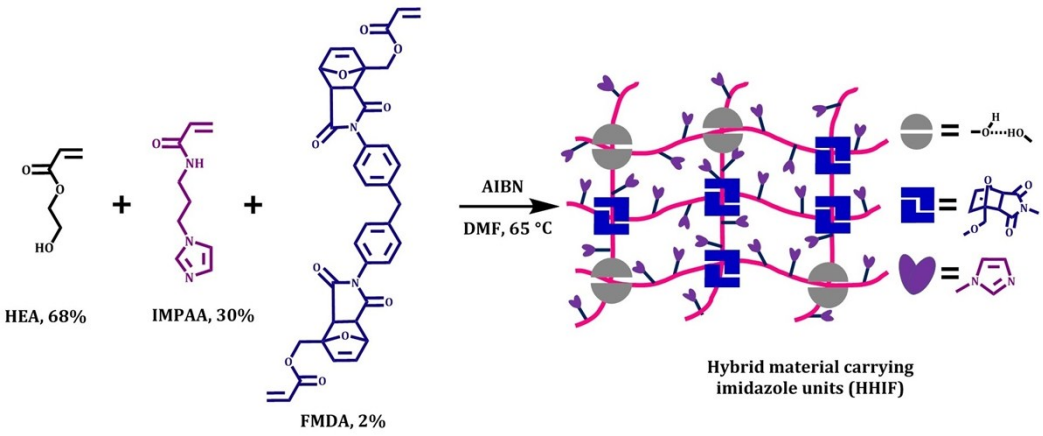

In a glass vial, HEA (2.32 g, 20 mmol, 68 mol%), IMPAA (1.58 g, 8.82 mmol, 30 mol%), FMDA (0.39 g, 0.59 mmol, 2 mol%) and AIBN (0.0429 g, 1 wt% w.r.t. total monomer) were gently blended. Next, 10 mL DMF was added and the reagents were homogeneously mixed. Then, the mixture was purged with N_2 for 10 min. Afterwards, the solution was transferred into a Teflon mold and heated at 65 °C for 12 h in a oven under nitrogen atmosphere. After polymerization, the materials was removed from the mold and washed with extensive ultrapure water and dichloromethane to remove residue monomer. Finally, the material was allowed to dry for 48 h at room temperature and followed by 48 h in a vacuum oven (100 torr) at 70 °C. The monomer conversion was determined by gravimetry to be about 92%.

Formation of HHIF-Zn material

The preparation of HHIF-Zn is through a submersion method according to the previous literature with a little modification[1]. Firstly, in a glass dish, 370 mg (10 mmol) of $Zn(OTf)_2$ was totally dissolved in 20 mL methyl alcohol, which can slightly swell HHIF, facilitating the penetration behavior of Zn^{2+} within polymeric network. Furthermore, methyl alcohol also has the ability to accelerate exchange rate of Zn^{2+}-imidazole bond, contributing to form stable metal-ligand crosslinks in solid states. Then, the as-prepared HHIF sample was immediately swollen in methyl alcohol solution, and kept submerged for 48 h. After completion, the obtained HHIF-Zn material was dried at 70 °C in a vacuum oven (100 torr) for 24 h before any measurement were performed. It should be note that all dry measurements were taken immediately after removing the samples from vacuum oven.

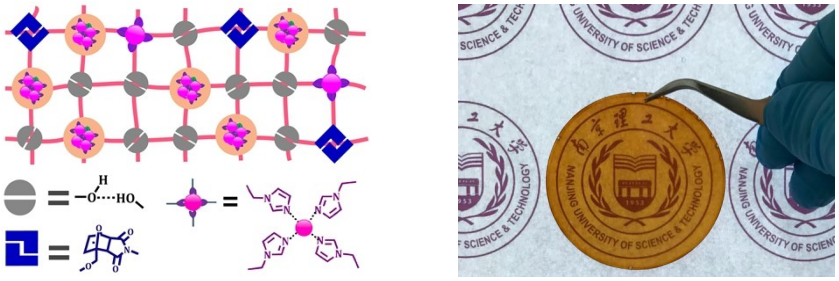

Fig. S5 Schematic illustration and optical photograph of the as-prepared HHIF-Zn sample.

Bulk Characterization

X-ray diffraction (XRD) patterns were carried out on a Bruker D8 Advanced diffractometer applying Cu Kα irradiation (λ=0.15406 Å). Attenuated total reflectance-FT-IR (ATR-FT-IR) spectra were recorded using a Bruker Tensor 27 Fourier transform-infrared spectrometer equipped with a Specac Golden Gate ATR heating cell in the range of 4000-600 cm^{-1}. Small angle X-ray scattering (SAXS) measurements on polymer samples were performed on Bruker AXS NanoSTAR equipped with a microfocus X-ray source, operating at λ=0.154 nm. Differential scanning calorimetry (DSC) measurement was performed at the heating rate of 20 °C min^{-1} with a TA DSC-25 differential scanning calorimeter from -70 °C to 200 °C. In the case of RH=95% sample, the second heating cycle is continuously followed by the first heating cycle to study the variation of the T_g values. Dynamic Vapor Sorption (DVS) was conducted on a TA VTI-SA Vapor sorption analyzer. Measurements were performed at different relative humidity from RH=0% to RH=95% with a interval of 5%. Inductively-coupled plasma atomic emission spectrometry (ICP-AES) was performed on a Thermo i CAPQ instrument. For scanning transmission electron (STEM) test, 100 nm thin cross-sections were sliced with Leica EM FC7 cryo-ultramicrotome at -100 °C, significantly below the glass transition temperature of the HHIF-Zn sample. STEM was performed in a high angle annular dark-field (HAADF-STEM) to check any distinct clustering of zinc atoms. Field emission scanning electron microscopy (FESEM) measurements were performed with a FEI Quanta 250FEG field emission electron microscope under an acceleration voltage of 20 kV for morphological observations. Optical microscopy images were performed by Jiangnan MV3000 optical microscope. The crosslinking density were detected using a magnetic resonance crosslinking density spectrometer (MRCDS, VTMR20-010V-T, Shanghai Niumag Corporation)

Relative Humidity control

We employed constant temperature humidity chamber (CTHC) to precisely control the relative humidity ranging from 20%-95% under 25 °C. After removing the HHIF-Zn sample from vacuum (70 °C, 100 torr), all dry measurements were carried out immediately. Instead, samples for mechanical measurements under different relative humidity (20%, 40%, 60%, 80% and 95%) were prepared as below. After drying at vacuum (70 °C, 100 torr), these samples were quickly transferred to CTHC, exposed to different relative humidity until reaching the water absorption equilibrium. Subsequently, the samples were immediately subjected to testing, including tensile testing, DMA testing, FT-IR and SAXS testing. Note that we try to ensure that the ambient humidity during the testing process is consistent with the water absorption equilibrium humidity of the materials.

Mechanical tests

Tensile tests were conducted using a Shimadzu AGS-X tester (500 N load cell) with a strain rate of 100 mm min^{-1}. Five samples with a tensile size of 15 mm gauge length × 5 mm width × 0.5 mm thickness were tested for each polymer sample, and the average value was given. For the cyclic tensile test, both loading and unloading process were performed at a strain rate of 100 mm min^{-1} at room temperature. Stress relaxation tests were measured by TA Q800 DMA using the tension mode. In stress-relaxation tests, the samples were quickly stretched to certain strain (5%, 100%) and then the strain was held constant and the time-dependent relaxation of stress was recorded. Relaxation time, τ^*, defined as the time for applied stress to reach 37% of its original value, is recorded to evaluate the dynamic feature of reversible interactions in HHIF-Zn network.[2] Bulk rheological measurements were carried out on a strain controlled rheometer on TA AR G2 Rheometer (20 mm parallel steel plate). Before testing, we cut the sample into a circular shape with diameter of 20 mm using a punch. Then, the circular sample was glued to the plates to avoid slippage.[3] Frequency sweeps were performed at a strain amplitude of 0.1% by varying the frequency between 0.1 Hz to 100 Hz at 25 °C. Impact test of HHIF-Zn at different relative humidities were tested according to ASTM D2794-93. The experiment was conducted via freely dropping a ball punch of 2 lbs weight from maximum height of 40 inch by using BYK gardener BYK-5546 impact tester.

Self-healing tests

For self-healing tests, the HHIF-Zn sample was cut into two completely separate pieces, and then the cut faces were gently pushed together for one minute. Next, the re-jointed film was transferred to oven with a healing temperature of 80 °C or gone through a dry-wet cycle (the redried condition of the wet sample: 35 °C, 100 torr). Subsequently, the self-healed sample was subject to tensile-stress test at room temperature at a strain rate of 100 mm min^{-1}. The healing efficiency, η, was quantitatively defined as the radio between the restored toughness relative to the original toughness.[4] The measurements were performed using three samples for each healing time to achieve the average value.

Supplementary figure

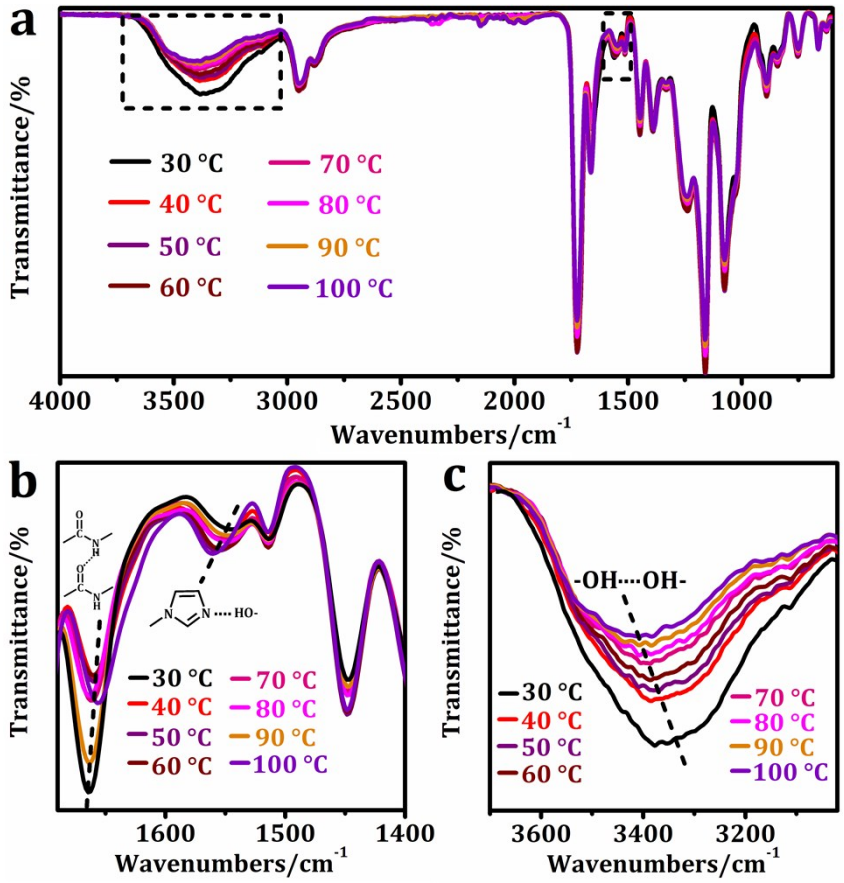

Fig. S6 Temperature-dependent FT-IR spectra of HHIF material heating from 30 °C to 100 °C. (a) full spectrum from 4000-600 cm^{-1}; (b) In the region of 1690-1400 cm^{-1}; (c) In the region of 3700-3020 cm^{-1}.

As shown in Fig. S6, for the temperature-dependent FT-IR spectra of HHIF film, there are three regions showing distinct changes with the increase of testing temperature. Specifically, when increasing the temperature, the -OH stretching signals from HEA (3370 cm^{-1}), and C=N stretching signals from imidazole groups (1560 cm^{-1}) are shifted towards higher wavenumbers whereas C=O signals from urethane groups (1654 cm^{-1}) are clearly shifted, indicating the dissociation of hydrogen bonds listed in Fig. S6 with the increase of temperature.[5]

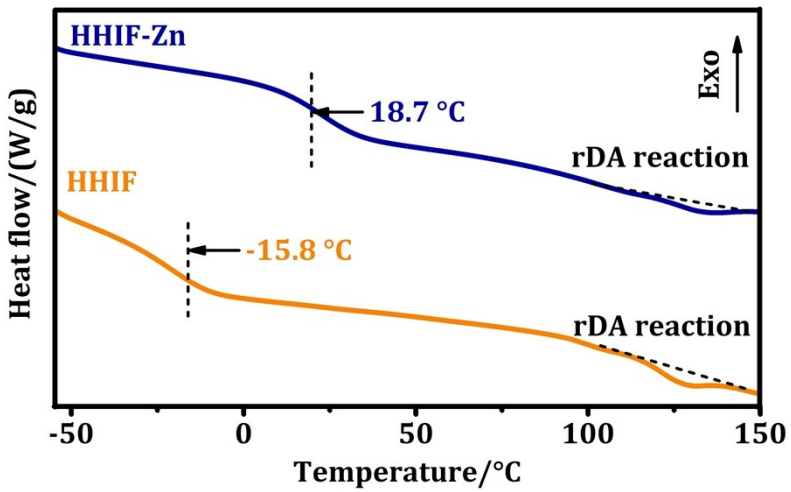

Fig. S7 DSC curves of HHIF and HHIF-Zn samples.

The thermal characteristics of HHIF and HHIF-Zn film were studied by DSC in the temperature range of -50 °C to 150 °C at a heating rate of 20 °C/min. For HHIF film, the glass transition temperature (T_g) is about -15.8 °C, which is close to that of virgin Polyhydroxyethyl acrylate (PHEA). However, after being swollen in Zn^{2+} solution, the T_g values of HHIF-Zn was increased up to 18.7 °C, suggesting the formation of Zn^{2+}-imidazole coordination bonds and corresponding ionic clusters, which lead to the increase of crosslinking density and then greatly restrict the movement of polymer chains. Thus, the T_g values is increased inevitably. Besides, a broad endo-thermic peak at about 127 °C exists within both HHIF and HHIF-Zn samples. This is assigned to the retro-DA reaction, indicating the existence of Diels-Alder bonds in polymer network.[6] No crystallization or melting peak is observed in DSC curves.

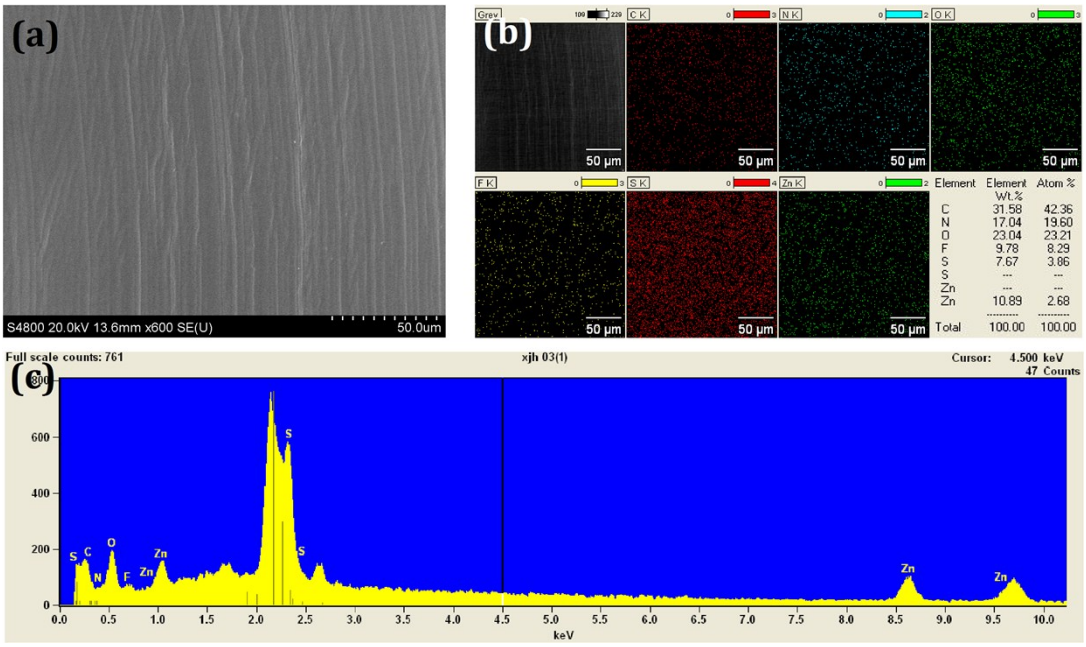

Fig. S8 (a) FESEM image of a cross sectional view of HHIF-Zn sample. (b) Elemental mapping images and (c) EDX spectrum of the selected region in section, manifesting the uniform distribution of Zn^{2+} in HHIF-Zn matrix.

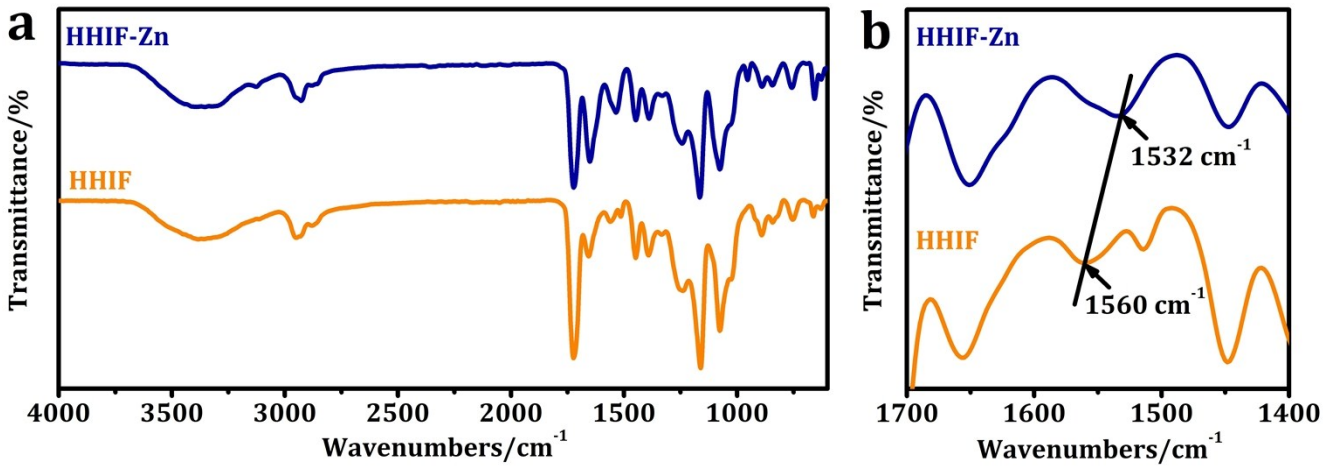

Fig. S9 FT-IR spectra of HHIF and HHIF-Zn samples; (a) full spectrum from 4000-600 cm^{-1}; (b) In the region of 1670-1400 cm^{-1}.

We employed FT-IR to examine the coordination interaction between Zn^{2+} and imidazole. As shown in HHIF spectrum, the absorption peak at 1560 cm^{-1}, corresponding to C=N characteristic vibration in imidazole ring is observed. However, upon coordinating with Zn^{2+}, this peak shifts to a low wavenumbers (1532 cm^{-1}), demonstrating the Zn^{2+}-imidazole coordination interaction.[7]

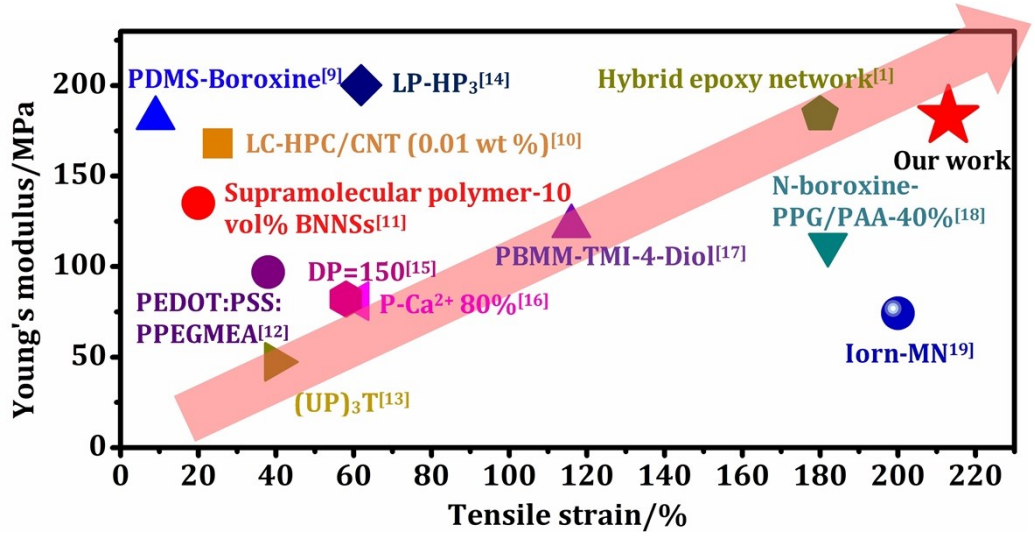

Fig. S10 Graphic comparison of Young's modulus and tensile strain values for some classical stiff polymer materials

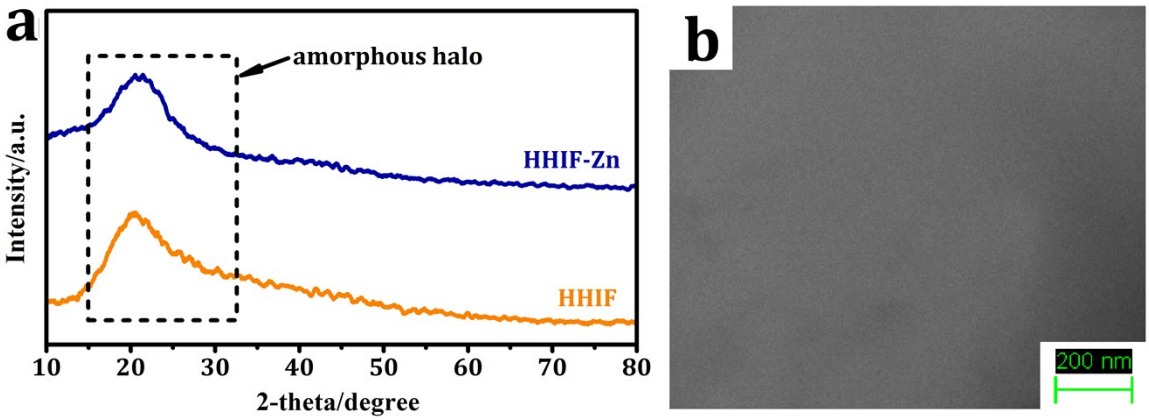

Fig. S11 (a) XRD curves of HHIF and HHIF-Zn samples. (b) HAADF-STEM image of HHIF-Zn sample.

As shown in Fig. S11a, the XRD curve of HHIF and HHIF-Zn films only displayed diffuse diffraction, suggesting the amorphous state at room temperature,[8] which is consistent with the DSC results. Thus, we can exclude the possibility of crystallization-induced mechanical reinforcement. Besides, HAADF-STEM (a technique with high atomic number sensitivity) was employed to investigate whether there are some zinc aggregates in HHIF-Zn matrix.[1] As shown in Fig. S11b, no zinc precipitate was detected in HAADF-STEM images, eliminating the possibility of nanofillers filling induced mechanical reinforcement.

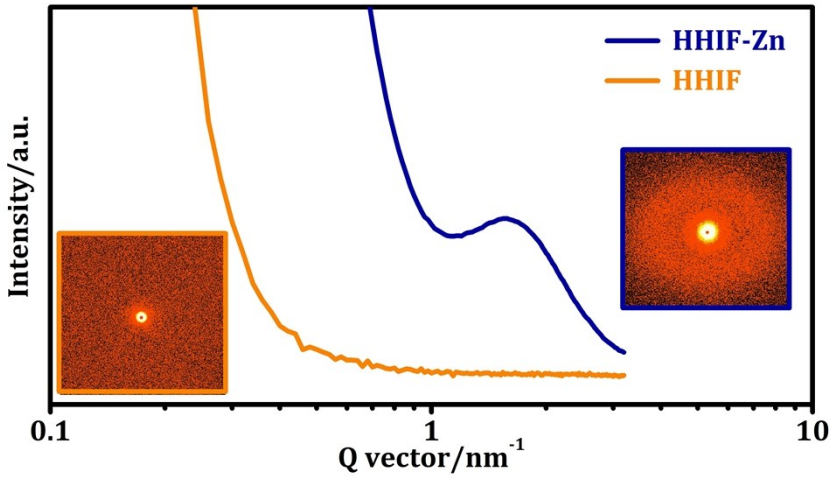

Fig. S12 SAXS diffraction of the HHIF and HHIF-Zn samples, insert picture showing the distinct two-dimension grazing-incidence small-angle X-ray scattering (2D-GISAXS) pattern of the corresponding samples.

As shown in Fig. S12, HHIF sample does not exhibit any scattering peak, whereas HHIF-Zn film shows a distinct signal at Q=1.65 nm^{-1} and the corresponding distance is calculated as 3.8 nm, stating the correlation distance (r) between zinc-rich metal-ligands crosslinked domains

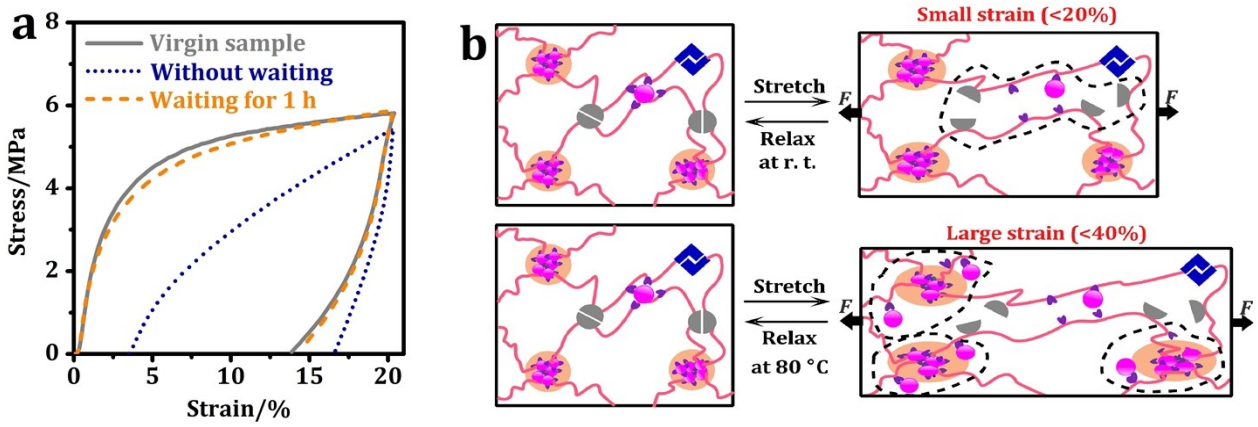

Fig. S13 (a) Sequential cyclic loading-unloading curves of HHIF-Zn samples with a tensile strain of 20%. (b) Schematic illustration of the proposed mechanism for the strain recovery.

At small strain (ε<20%), the generated residual strain could be decreased to zero with 1 h relaxation time. This result suggests that the partially broken noncovalent bonds, including hydrogen bonds and coordination bonds, are able to reform after tensile fracture. However, when the applied strain is beyond 40%, the HHIF-Zn sample cannot return back its original length (with a notable residual strain) after relaxing for 6 h at room temperature. Interestingly, higher relaxation temperature (80 °C) leads to the fully restoration of the residual strain within 30 min. This phenomenon is attributed to partial broken of ionic clusters, which need external energy to restore themselves.

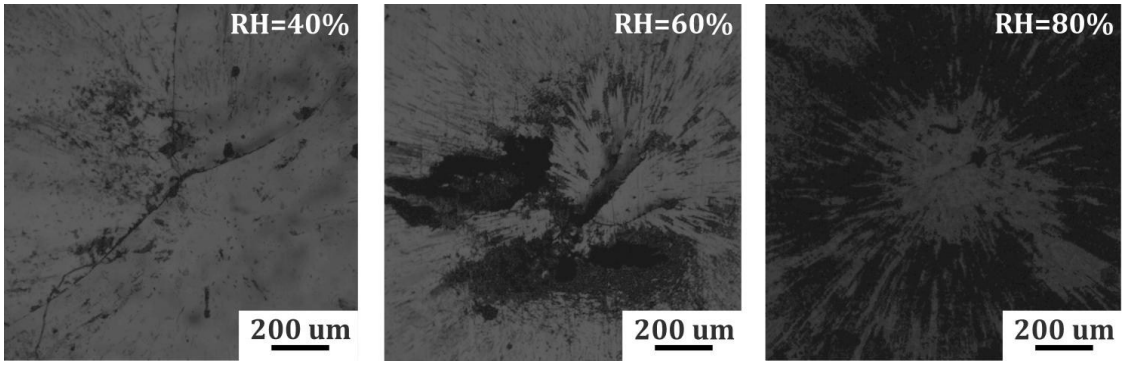

Fig. S14 Standard ball-drop tests of HHIF-Zn (RH=40%, RH=60%, RH=80%) samples. All the samples emerge visible cracks and flakes upon impacting.

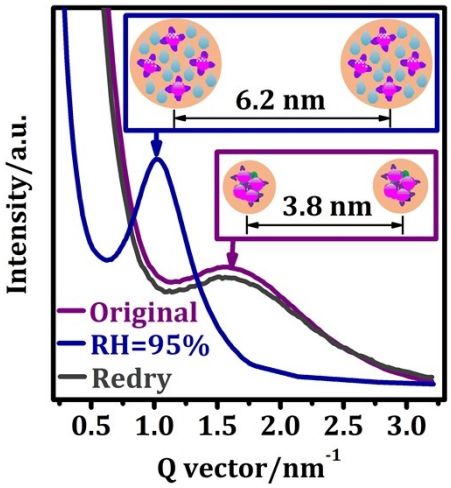

Fig. S15 SAXS diffraction of HHIF-Zn (original, RH=95%, Redried); insert pictures record the change of corresponding distance and size of the ionic clusters.

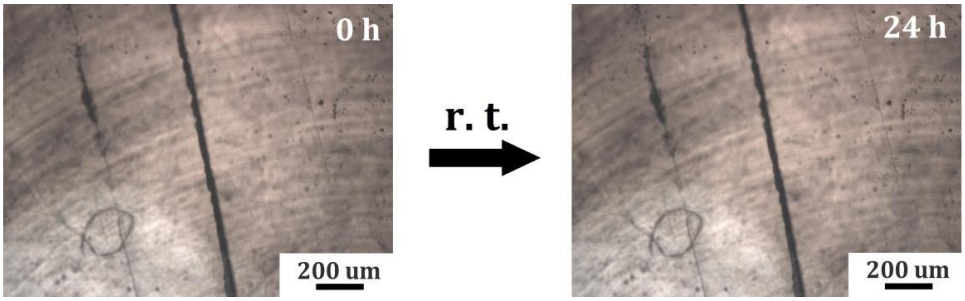

Fig. S16 Optical microscope images recording the self-healing process of HHIF-Zn sample at room temperature. The scratches exhibit no distinct changes upon healing at r. t. for 24 h.

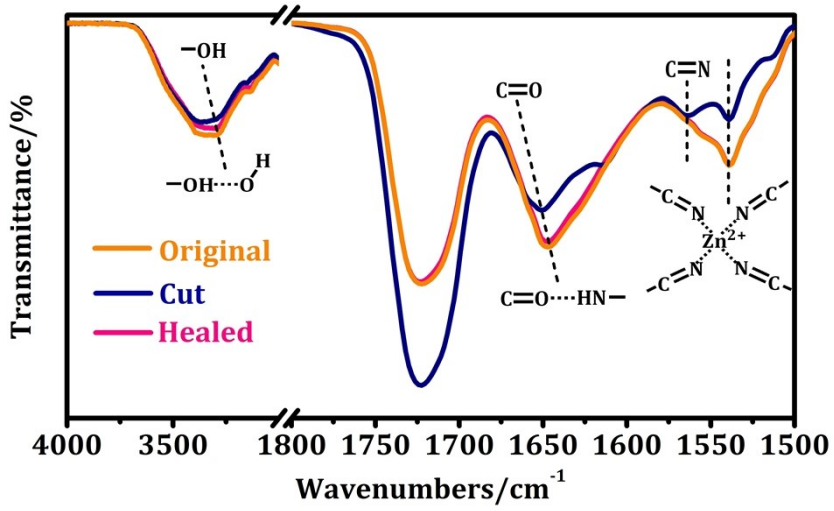

Fig. S17 FT-IR spectra collected from undamaged, damaged and healed areas as a function of healing temperature for 80 °C.

As shown in Fig. S17, the absorption band at 1654 cm^{-1} assigned to stretching vibration of hydrogen-bonded C=O from urethane groups shits to high wavenumbers area (red shift) upon mechanical damage, and the absorption band centered at 3370 cm^{-1} corresponding to the stretching vibration of hydrogen-bonded -OH/-NH also generate the red shift. These prominent spectroscopic changes indicate the initially hydrogen bonds partially dissociate after being damaged. However, after healing at 80 °C for 5 h, these changed bands almost return to their original location, manifesting the recombination of dissociated hydrogen bonds. Similarly, the band at 1532 cm^{-1} assigned to stretching vibration of coordinated C=N from imidazole groups changes as well. Specifically, upon suffering from damage, the intensity of the coordinated C=N bond decrease, whereas the intensity of the free C=N bond subsequently increase. These suggest that Zn^{2+}-imidazole coordination bonds are partially dissociate after being damaged. However, these bands return to its original state after healing for 5 h at 80 °C, indicating the reformation of destructive coordination bonds.

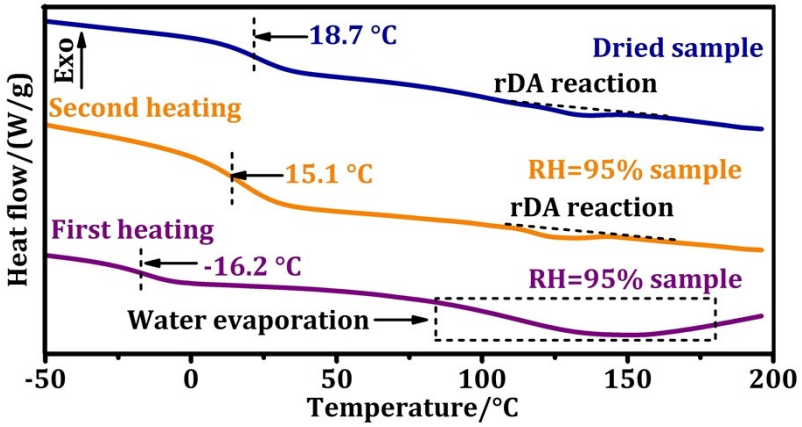

Fig. S18 DSC curves of the HHIF-Zn sample. Purple line: first heating process of the RH=95% sample; bronzing line: second heating process of the RH=95% sample; green line: first heating line of the dried HHIF-Zn sample.

As shown in Fig. S18, the T_g value of the RH=95% sample in the first heating process is about -16 °C, whereas it increases up to 15.1 °C in the continuous second heating process, reaching the T_g value of the dried HHIF-Zn film (18.7 °C). Meanwhile, the big endothermic peak of RH=95% sample in the first heating process, corresponding to the water evaporation, has been changed to a small endothermic peak of rDA reaction in the continuous second heating process. These phenomenon strongly demonstrating that water molecule can penetrate into the HHIF-Zn network to weaken the non-covalent interactions, facilitating the sufficient movement of the polymer chains.[13]

Supplementary Table

Table. S1 Comparison of the increased amplitudes of mechanical properties for HHIF-Zn with others

Sample	Increased amplitudes/a.u.		
	Young's modulus	Tensile strength	Toughness
Hybrid epoxy network[1]	770	58	92
Iron-MN[19]	12	7	10
SPU (0.50:0.50)[20]	6.5	2.8	4.6
SN[21]	3.5	/	100
VPR-0.67[22]	3.6	6.9	5.1
PAAm-CNF-0.5-Cs^{3+}[23]	102.8	31.4	168
CNF-PEG 15[24]	11.9	5.2	14.8
EZ2F3[25]	47	2	3
PAA-CNF-Fe^{3+}-1.00[26]	51.1	27.8	3.6
IPN[27]	2.5	1.9	1.5
P(HEMA-*co*-UPyMA)/OxMWCNT-*g*-UPy[28]	4.2	1.5	1
VDT 66.7%[29]	/	6	/
SSBR-TAD-5.32[30]	/	2.2	2.6
ACON[31]	0.93	1.3	7.4
PDG/PAAm [bilayer][32]	/	15.8	/
PU/LGO[33]	89	1.5	2.6
PU_{20}-*b*-P(D_{320}-r-U_{40})-*b*-PU_{20}[34]	4.25	16.3	36.5
dGO-PVA (D:GO=0.5:1)[35]	1.4	2	/
g-IR-3-2.5[36]	2.6	1.9	2
PUU-*g*-C_3N_4 NSs-2.0[4]	2.2	2.5	2
PU-2wt%GO[37]	2	1.5	/
Alginate-polyacrylamide[38]	3.6	42.2	

Table. S2 Summary of the crosslinking densities for HHIF and HHIF-Zn film

Sample	Crosslinking density/(mol/cm^3)
HHIF	$2.11\pm0.08\times10^{-4}$
HHIF-Zn	$4.86\pm0.29\times10^{-4}$

Table. S3 Summary of the mechanical properties for HHIF-Zn sample under different humidities.[a]

Sample	Young's modulus/MPa[b]	Tensile strength/MPa	Tensile strain/%	Toughness/(MJ/m^3)[c]
Original dried film	183±12	13.49±0.61	213±3	20.07±2.06
RH=20%	123±9	10.55±0.44	202±5	14.47±1.48
RH=40%	84±8	6.81±0.35	190±4	9.19±1.02
RH=60%	42±5	4.71±0.19	183±4	5.73±0.61
RH=80%	21±2	3.01±0.16	173±5	2.88±0.32
RH=95%	1.7±0.1	1.01±0.08	148±6	0.76±0.13

[a] Strain rate = 100 mm· min^{-1}, 25 °C. [b] Young's modulus is calculated from the initial slope of stress-strain curves. [c] Toughness is calculated by manually integrating the area under the stress-strain curve.

Table. S4 Summary of the mechanical and self-healing properties for HHIF-Zn sample healed at 80 °C.[a]

Sample	Young's modulus/MPa[b]	Tensile strength/MPa	Tensile strain/%	Toughness/(MJ/m^3)[c]	Self-healing efficiency (%)[d]
Original dried film	183±12	13.49±0.61	213±3	20.07±2.06	94.77
Healed at 80 °C	181±13	12.43±0.55	209±4	19.02±2.19	

[a] Strain rate = 100 mm· min^{-1}, 25 °C. [b] Young's modulus is calculated from the initial slope of stress-strain curves. [c] Toughness is calculated by manually integrating the area under the stress-strain curve. [d] Self-healing efficiency is calculated from the ratio of toughenss of healed samples to that virgin sample.

Table. S5 Summary of the mechanical and self-healing properties for HHIF-Zn sample healed by a water-assisted healing method.[a]

Sample	Young's modulus/MPa[b]	Tensile strength/MPa	Tensile strain/%	Toughness/(MJ/m^3)[c]	Self-healing efficiency (%)[d]
Original RH=95% film	1.7±0.1	1.01±0.08	148±6	0.76±0.13	/
Healed at RH=95%, 6 h	1.56±0.08	0.35±0.02	46±2	0.11±0.02	14.47%
Healed at RH=95%, 12 h	1.61±0.12	0.61±0.05	90±3	0.29±0.05	38.16%
Healed at RH=95%, 24 h	1.68±0.09	0.98±0.09	146±5	0.74±0.15	97.37%
Original dried film	183±12	13.49±0.61	213±3	20.07±2.06	/
Healed at RH=95% for 24 h and redried film[e]	180±12	11.89±0.49	208±4	17.16±1.26	85.50%

[a] Strain rate = 100 mm· min^{-1}, 25 °C. [b] Young's modulus is calculated from the initial slope of stress-strain curves. [c] Toughness is calculated by manually integrating the area under the stress-strain curve. [d] Self-healing efficiency is calculated from the ratio of tensile strength of healed samples to that virgin sample. [e] The film is dried at 35 °C with a pressure of 100 torr.

Supplementary movie

Movie. S1: This movie showed that the dried HHIF-Zn sample is hard enough to easily penetrate gelatin, whereas the soft water-containing sample (RH=95%) is unable to achieve this goal.

References

[1] E. Filippidi, T. R. Cristiani, C. D. Eisenbach, J. H. Waite, J. N. Israelachvili, B. K. Ahn, M. T. Valentine, *Science* **2018**, 358, 502-505.
[2] Z. P. Zhang, M. Z. Rong, M. Q. Zhang, *Adv. Funct. Mater.* **2018**, 28, 1706050.
[3] J. R. Wu, L. H. Cai, D. A. Weitz, *Adv. Mater.* **2017**, 29, 1702616.
[4] J. H. Xu, S. Ye, C. D. Ding, L. H. Tan, J. J. Fu, *J. Mater. Chem. A* **2018**, *6*, 5887-5898.
[5] P. Cordier, F. Tournilhac, C. Soulié-Ziakovic, L. Leibler, *Science* **2008**, 451, 977-980.
[6] N .B. Pramanik, G. B. Nando, N. K. Singha, *Polymer* **2008**, 69, 349-356.
[7] S. F. Wang, Y. Liu, M. W. Zhang, D. D. Shi, Y. F. Li, D. D. Peng, G. W. He, H. Wu, J. F. Chen, Z. Y. Jiang, *J. Membrane Sci.* **2016**, 505, 44-52.
[8] D. W. R. Balkenende, C. A. Monnier, G. L. Fiore, C. Weder, *Nat. Commun.* **2016**, 7, 10995.
[9] J. C. Lai, J. F. Mei, X. Y. Jia, C. H. Li, X. Z. You, Z. N. Bao, *Adv. Mater.* **2016**, 28, 8277-8282.
[10] C. Echeverria, L. E. Aguirre, E. G. Merino, P. L. Almeida, M. H. Godinho, *ACS Appl. Mater. Interfaces* **2015**, 7, 21005-21009.
[11] L. X. Xing, Q. Li, G. Z Zhang, X. S. Zhang, F. H. Li, L. Liu, Y. D. Huang, Q. Wang, *Adv. Funct. Mater.* **2016**, 26, 3524-3531.
[12] L. V. Kayser, M. D. Russell, D. Rodriquez, S. N. Abuhamdeih, C. Dhong, S. Khan, A. N. Stein, J. Ramirez, D. J. Lipomi, *Chem. Mater.* **2018**, 30, 4459-4468.
[13] M. J. Liu, P. Liu, G. Lu, Z. T. Xu, X. Yao, *Angew. Chem. Int. Ed.* **2018**, DOI: 4459-4468.10.1002/ange.201805206.
[14] Y. H. Zhang, L. Yuan, Q. B. Guan, G. Z. Liang, A. J. Gu, *J. Mater. Chem. A* **2017**, 5, 16889-16897.
[15] G. A. Williams, R. Ishige, O. R. Cromwell, J. Chung, A. Takahara, Z. B. Guan, *Adv. Mater.* **2015**, 27, 3934-3941.
[16] J. C. Li, H. Ejima, N. Yoshie, *ACS Appl. Mater. Interfaces* **2016**, 8, 19047-19053.
[17] K. H. Wu, L. F. Feng, X. P. Gu, C. L. Zhang, S. Shen, *Ind. Eng. Chem. Res.* **2018**, 57, 946-953.
[18] C. Y. Bao, Y. J. Jiang, H. Y. Zhang, X. Y. Lu, J. Q. Sun, *Adv. Funct. Mater.* **2018**, 28, 1800560.
[19] X. H. Zhang, J. Liu, Z. Y. Zhang, S. W. Wu, Z. H. Tang, B. C. Guo, L. Q. Zhang, *ACS Appl. Mater. Interfaces* **2018**, 10, 23485-23489.
[20] H. Daemi, S. Rajabi-Zeleti, H. Sardon, M. Barikani, A. Khademhosseini, H. Baharvans, *Biomaterials* **2016**, 84, 54-63.
[21] E. Ducrot, Y. L. Chen, M. Bulters, R. P. Sijbesma, C. Creton, *Science* **2014**, 344, 186-189.
[22] Z. H. Tang, J. Huang, B. C. Guo, L. Q. Zhang, F. Liu, *Macromolecules* **2016**, *49*, 1781-1789.
[23] J. Yang, F. Xu, C. R. Han, *Biomacromolecules* **2017**, *18*, 1019-1028
[24] J. Yang, M. G. Ma, X. M. Zhang, F. Xu, *Macromolecules* **2016**, *49*, 4340-4348.
[25] X. H. Zhang, Z. H. Tang, B. C. Guo, L. Q. Zhang, *ACS Appl. Mater. Interfaces* **2016**, *8*, 32520-32527.
[26] C. Y. Shao, H. L. Chang, M. Wang, F. Xu, J. Yang, *ACS Appl. Mater. Interfaces* **2017**, *9*, 28305-28318.
[27] E. M. Foster, E. E. Lensmeyer, B. Zhang, P. Chakma, J. A. Flum, J. J. Via, J. L. Sparks, D. Konkolewicz, *ACS Macro Lett.* **2017**, *6*, 495-499.
[28] T. T. T. Myllymaki, L. Lemetti, Nonappa, O. Ikkala, *ACS Macro Lett.* **2017**, *6*, 210-214.
[29] J. L. Zhang, N. Wang, W. G. Liu, X. L. Zhao, W. Lu, *Soft Matter* **2013**, *9*, 6331-6337.
[30] J. Huang, L. J. Zhang, Z. H. Tang, S. W. Wu, N. Y. Ning, H. B. Sun, B. C. Guo, *Macromol. Rapid Commun.* **2017**, *38*,1600678.
[31] J. A. Neal, D. Mozhdehi, Z. B. Guan, *J. Am. Chem. Soc.* **2015**, *137*, 4846-4850.
[32] M. A. Haque, T. Kurokawa, G. Kamita, J. P. Gong, *Macromolecules* **2011**, *44*, 8916-8924.
[33] M. Z. Seyedin, J. M. Razal, P. C. Innis, R. Jalili, G. G. Wallace, *Adv. Funct. Mater.* **2015**, *25*, 94-104.
[34] S. Yoshida, H. Ejima, N. Yoshie, *Adv. Funct. Mater.* **2017**, *27*, 1701670.
[35] S. H. Hwang, D. W. Kang, R. S. Ruoff, H. S. Shin, Y. B. Park, *ACS Nano*. **2014**, *8*, 6739-6747.
[36] S.W. Wu, M. Qiu, Z. H. Tang, J. Lu, B. C. Guo, *Macromolecules* **2017**, *50*, 3244-3253.
[37] Z. X. Chen, H. B. Lu, *J. Mater. Chem. A* **2012**, *22*, 12479-12490.
[38] J. Y. Sun, X. H. Zhao, W. R. K. Illeperuma, O. Chaudhuri, K. H. Oh, D. J. Mooney, J. J. Vlassak, Z. G. Suo, *Nature* **2012**, *489*, 133-136.